Composites: Part A 180 (2024) 108082

Contents lists available at ScienceDirect

Composites Part A

journal homepage: www.elsevier.com/locate/compositesa

On the surface characteristics and removability of RB-SiC composite processed by nanosecond pulsed laser

Hong An [a], Yongfeng Qian [a,*], Lin Zhang [b], Zhiyu Zhang [c], Hu Huang [a,*], Jiwang Yan [b]

[a] Key Laboratory of CNC Equipment Reliability, Ministry of Education, School of Mechanical and Aerospace Engineering, Electron Microscopy Center, Jilin University, Changchun 130022, China
[b] Department of Mechanical Engineering, Faculty of Science and Technology, Keio University, Yokohama 223-8522, Japan
[c] Key Laboratory of Optical System Advanced Manufacturing Technology, Changchun Institute of Optics, Fine Mechanics and Physics, Chinese Academy of Sciences, Changchun 130033, China

ARTICLE INFO

Keywords:
A. Ceramic-matrix composites (CMCs)
B. Hardness
D. Surface analysis
E. Surface treatments

ABSTRACT

The inherent hard-brittle nature of RB-SiC composite poses significant challenges for efficient machining, hindering its application and promotion. Laser processing is a non-contact treatment technique that can effectively modify the mechanical properties of the material surface, thereby altering its removability. Accordingly, the change in surface characteristics of RB-SiC composite induced by nanosecond laser irradiation was investigated. It was found that laser irradiation could effectively soften the RB-SiC composite (with a maximum reduction in hardness by 40.7%), and the softening degree was strongly dependent on the laser parameters. The chemical composition analysis showed that the SiC content was decreased while the Si content was increased after laser irradiation, which was mainly responsible for the hardness reduction of RB-SiC composite. In addition, compared to the original RB-SiC composite, the laser-irradiated samples exhibited enhanced weight loss during the polishing process. This work gives a feasible route to improve the removability of RB-SiC composite.

1. Introduction

Reaction-bonded silicon carbide (RB-SiC), as an advanced ceramic material, is produced through a manufacturing process that involves the infiltration of liquid silicon (Si) into porous SiC/C billets at high temperatures, resulting in the formation of a composite material consisting of the original SiC, newly formed SiC and residual Si [1–3]. Due to its remarkable mechanical, physical and chemical properties, such as excellent wear and corrosion resistance, high specific stiffness and outstanding thermal stability, RB-SiC is considered as one of the most promising materials for space mirrors and has been extensively used in space optics, aerospace, military and other cutting-edge fields [4–6]. However, its inherent characteristics of high hardness and brittleness bring enormous challenges such as low processing efficiency, severe tool wear and high processing cost to RB-SiC in the machining process, which greatly hinders its practical engineering applications [7–9]. Therefore, improving the machinability of RB-SiC composite has become an inevitable research trend.

It has been well demonstrated that reducing the surface hardness of the material can effectively enhance the machinability [10–12]. In one previous study [13], by using Murakami's reagent in chemical assisted shape adaptive grinding, a thin passivation layer with a relatively low hardness was formed on the top of the WC-Co coating, thus facilitating material removal during the grinding process. Similarly, the addition of ethylenediamine during the friction process between the fixed abrasive pad (FAP) and the silica glass under deionized water polishing slurry condition promoted the formation of a softened layer, which ultimately led to a high material removal rate [14]. In addition to chemical methods, thermal-assisted techniques have also been developed and applied to improve the machinability of difficult-to-machine materials [15]. Liu et al. [16] compared the mechanical properties of KH_2PO_4 (KDP) crystal at ambient and elevated temperatures, and the experimental results indicated that the hardness of KDP crystal at elevated temperature (i.e. 160 °C) was significantly reduced by 21.4 % compared with that at ambient temperature (i.e. 23 °C), and accordingly, the ductile deformation capacity was increased, implying a high machinability at elevated temperature. However, the aforementioned methods may be not suitable for softening the RB-SiC composite. Due to the excellent chemical resistance, it is quite challenging to select suitable chemical reagents to soften the RB-SiC surface [17]. In addition, the

* Corresponding authors.
E-mail addresses: qianyf@jlu.edu.cn (Y. Qian), huanghu@jlu.edu.cn (H. Huang).

https://doi.org/10.1016/j.compositesa.2024.108082
Received 26 October 2023; Received in revised form 22 January 2024; Accepted 7 February 2024
Available online 10 February 2024

melting points of Si and SiC contained in RB-SiC composite are very high and vastly different, making it difficult to process RB-SiC composite through conventional thermal treatment techniques [18–21].

Currently, laser processing, as an emerging surface modification technology, offers a range of distinctive advantages, including non-contact machining without tool wear, simple operation, easy maintenance and a high degree of flexibility, has been extensity used to modify the mechanical properties of various materials [22–26]. In particular, the chemical composition of the material surface can be changed by laser-induced chemical reactions, enabling the change in surface hardness. For example, femtosecond laser irradiation could induce surface graphitization of SiC materials, resulting in a significant decrease in their surface hardness [27]. After laser surface melting (LSM) of gas-nitrided P20 steel using a continuous laser, the surface nitrided layer underwent a denitrification reaction, consequently leading to a reduction in its surface hardness [28]. For RB-SiC composite, laser irradiation could induce the decomposition of the SiC particles within them, leading to the formation of a recast layer with a relatively low hardness on the top of the RB-SiC substrate. However, as a two-phase composite material, the interaction processes and mechanisms between laser and RB-SiC composite are highly intricate and multifaceted, and the evolution of the surface characteristics and mechanical properties of RB-SiC composite induced by laser irradiation has not been fully revealed. Moreover, the effects of the mechanical property changes on the removability of RB-SiC composite also need to be elucidated urgently.

For bridging this gap, this study aims to investigate the evolution of the surface characteristics of RB-SiC composite induced by nanosecond laser irradiation. The effects of laser parameters (i.e. laser power and scanning speed) on the micro-morphologies, chemical compositions and hardness of the laser-irradiated regions were comprehensively studied. To investigate the influence of laser-induced surface characteristic changes on the removability, material removal behaviors of the original and laser-irradiated samples during the mechanical polishing process were comparatively investigated. Correspondingly, the mechanisms responsible for the laser-induced changes in surface characteristics and removability were elucidated and clarified. The presented work deepens the understanding of the interaction processes and mechanisms between laser and RB-SiC composite, and contributes to the development of advanced thermal-assisted setups/methods for achieving efficient processing of RB-SiC composite.

2. Materials and experiments

2.1. Materials

The RB-SiC samples utilized in experiments are cuboid-shaped with dimensions of 20 × 20 × 2 mm^3 (length × width × thickness). To probe the distribution of SiC and Si phases within the RB-SiC composite, the samples underwent a mechanical polishing process using 0.5 μm diamond polishing paste until a relatively smooth surface (with a surface roughness (*Sa*) of about 100 nm) was obtained. Prior to microscopic observation, the polished RB-SiC samples were thoroughly cleaned with 95 % ethanol. The scanning electron microscope (SEM) image of the RB-SiC composite is presented in Fig. 1(a), where the gray regions represent SiC particles and the white region represents the Si matrix. To further confirm the phase composition, Raman spectroscopy tests (DXR3, Thermo Fisher Scientific) were performed on the gray and white regions, respectively, and the results are shown in Fig. 1(b). The Raman spectral curve of the white region exhibits a prominent peak at approximately 520 cm^{-1}, which is assigned to the monocrystalline Si [29]. For gray regions, two prominent peaks are observed at approximately 788 and 969 cm^{-1}, both of which correspond to the SiC phases [30].

2.2. Experimental device and processing conditions

During experiments, a nanosecond laser micro-fabrication system which includes a fiber pulsed laser source (SP-050P-A-EP-Z-F-Y, SPI Lasers, UK) with a laser wavelength of 1064 nm and a pulse width of 7 ns, a F-theta lens with a focused length of 160 mm, and a pair of optical reflecting mirrors was used to irradiate the RB-SiC surface. During laser irradiation, the laser beam was directed by the optical reflecting mirrors, and then focused onto the RB-SiC surface through the F-theta lens, producing a circular Gaussian spot with a diameter of about 43 μm. Two sets of comparative experiments were designed to investigate the evolution of surface characteristics induced by nanosecond pulsed laser irradiation. In one set, the laser power was varied while keeping the other parameters constant, whereas in the other set, the laser scanning speed was varied while maintaining the other parameters at a constant value. All laser irradiation experiments were performed at room temperature under atmospheric conditions. Table 1 lists the detailed laser irradiation conditions used.

Table 1
Laser irradiation conditions.

Laser parameter	Value
Wavelength (nm)	1064
Pulse width (ns)	7
Power (W)	4.0, 14.7, 22.0
Scanning speed (mm/s)	10, 40, 60
Repetition frequency (kHz)	700
Spot size (μm)	~ 43

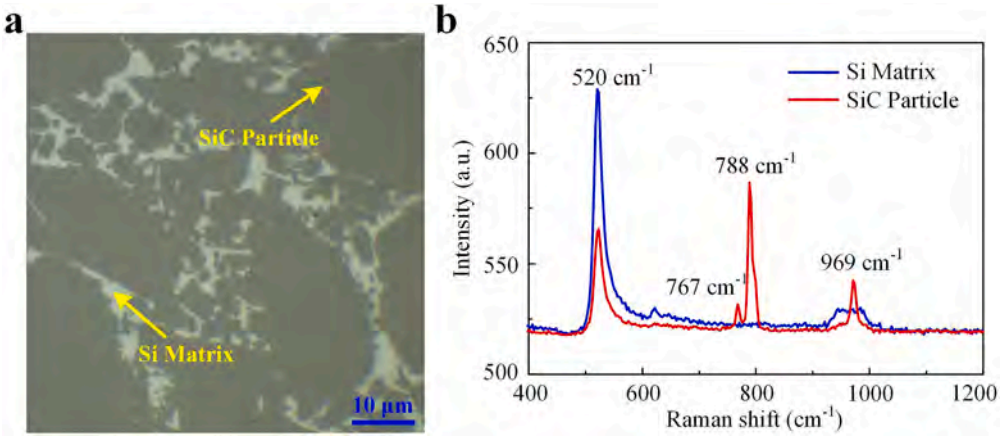

Fig. 1. (a) SEM image and (b) Raman spectral curves of the RB-SiC composite.

2.3. Measurement and characterization methods

The micro-morphologies of the laser-irradiated regions were characterized using a tungsten filament scanning electron microscope (SEM, JSM-IT500A, JEOL). A white light interferometer (NewView 8000, Zygo) was employed to acquire the three-dimensional (3D) profiles of the laser-irradiated regions. The elemental distribution and phase composition of the original and laser-irradiated surfaces were characterized by an energy dispersive X-ray spectrometer (EDS, EX-74600U4L2Q, JEOL) and a X-ray diffractometer (XRD, D8 Advance, Bruker), respectively. Prior to the hardness test, the laser-irradiated surfaces were mechanically polished to obtain relatively flat surface regions. Nanoindentation tests were performed on these relatively flat regions as well as on the original RB-SiC surface to investigate possible hardness changes induced by nanosecond laser irradiation. The nanoindentation tests were carried out in load-controlled mode using a nanoindentation instrument (DUH-211S, Shimadzu) equipped with a triangular pyramid diamond indenter, and a maximum indentation load of 50 mN with a constant loading rate of 5 mN/s was employed. After the nanoindentation tests, the micro-morphologies and 3D profiles of the residual indents were captured by SEM and atomic force microscopy (AFM, Dimension Icon), respectively.

3. Results and discussion

3.1. Surface microstructure and hardness

Fig. 2 presents the SEM micrographs of the laser-irradiated regions obtained at various power levels. The used scanning speed is fixed at 10 mm/s. When the RB-SiC surface is exposed to laser irradiation at a relatively low power of 4.0 W, no obvious laser scanning traces are observed, with localized small-scale pits being the predominant characteristics, as shown in Fig. 2(a). When the laser power is increased to 14.7 W, uniform micro-cone structures appear on the laser-irradiated region and they become more pronounced with the further increase of laser power (see Fig. 2(b) and (c)). In addition, these micro-cone structures are covered by porous spider web-like film of varying extents, as illustrated in the insets of Fig. 2(b) and (c). Since the laser-irradiated surfaces shown in Fig. 2(a)-(c) are relatively rough, they were mechanically polished to obtain relatively flat regions prior to nanoindentation tests. Fig. 2(d)-(f) presents the SEM micrographs of the laser-irradiated regions after polishing. In Fig. 2(d), the laser-irradiated region after polishing exhibits a similar morphology to that of the original RB-SiC surface shown in Fig. 1(a) (i.e. gray SiC particles embedded in the white Si matrix), which indicates that the interaction between RB-SiC composite and laser is very weak when laser irradiation is performed at a relatively low power. In contrast, the laser-irradiated regions after polishing shown in Fig. 2(e) and (f) are covered by laser scanning traces being parallel to each other as well as many smooth regions, confirming that a strong interaction between laser and RB-SiC composite at relatively high powers.

Fig. 3(a) and (b) presents the SEM micrographs of the laser-irradiated regions obtained under a constant laser power of 14.7 W and various scanning speeds, and Fig. 3(c) and (d) shows the SEM micrographs of these laser-irradiated regions after polishing. Compared to Fig. 2(b), when increasing the scanning speed from 10 mm/s to 40 mm/s or more (see Fig. 3(a) and (b)), the resulting laser-irradiated regions are free of

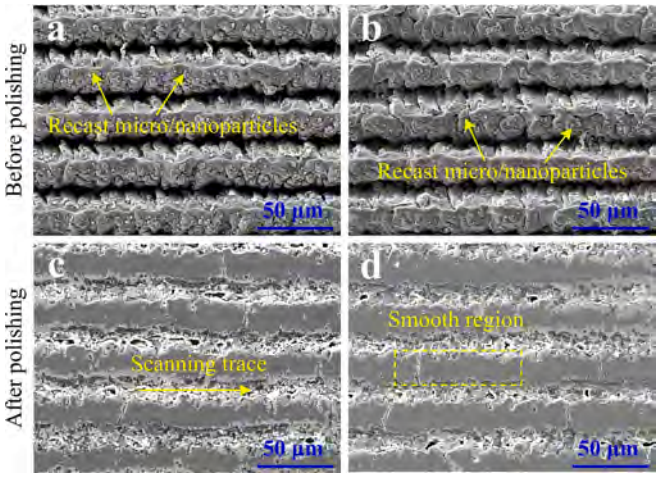

Fig. 3. SEM micrographs of the laser-irradiated regions obtained at various scanning speeds: (a) 40 mm/s, and (b) 60 mm/s. (c) and (d) SEM micrographs of the laser-irradiated regions after polishing, corresponding to different conditions in Fig. 3(a) and (b).

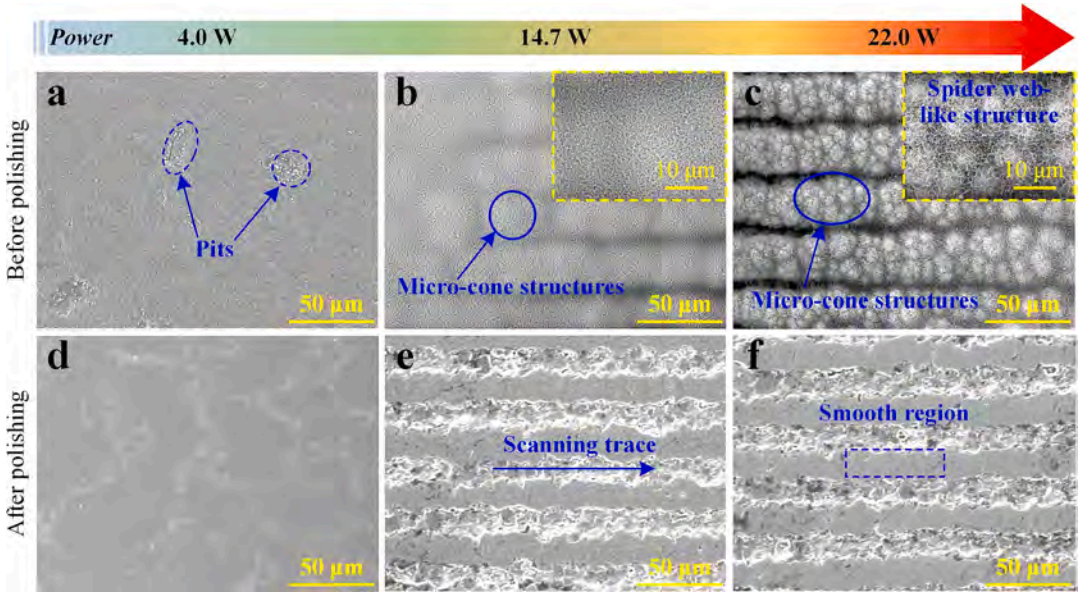

Fig. 2. SEM micrographs of the laser-irradiated regions obtained at various power levels: (a) 4.0 W, (b) 14.7 W, and (c) 22.0 W. (d)-(f) SEM micrographs of the laser-irradiated regions after polishing, corresponding to different conditions in Fig. 2(a)-(c).

porous spider web-like film, but they are still covered with micro-cone structures accompanied by a large number of recast micro/nano-particles. In addition, as illustrated in Fig. 3(c) and (d), these laser-irradiated regions after polishing exhibit micro-morphologies similar to those shown in Fig. 2(e) and (f), which is characterized by a uniform alternation between laser scanning traces and lath-shaped smooth regions.

Fig. 4 presents the 3D profiles of the original RB-SiC surface and polished laser-irradiated regions. In Fig. 4(b), it is seen that nanosecond laser irradiation with a relatively low power of 4.0 W does not cause serious damage to the RB-SiC composite, and the resulting laser-irradiated region exhibits relatively smooth topography after mechanical polishing. In contrast, the laser-irradiated regions obtained under other irradiation conditions have only partially smooth regions after polishing, as illustrated in Fig. 4(c)-(f). The width of these lath-shaped smooth regions between adjacent laser scanning traces all exceeds 20 μm, and the nanoindentation tests were performed around the center of these smooth regions. Fig. 5 illustrates the SEM morphologies of the representative residual indents formed on the original RB-SiC surface and laser-irradiated regions. It is clearly seen that the dimensions of the residual indents formed on the laser-irradiated regions are larger than that on the original RB-SiC surface, which indicates that the resistance of RB-SiC composite to plastic deformation is weakened after nanosecond laser irradiation.

Fig. 6(a)-(e) presents the AFM images of the residual indents corresponding to Fig. 5(b)-(f). According to Figs. 5 and 6, the evident changes are that the side length and depth of the triangular residual indent formed on the laser-irradiated regions exhibit a gradual increasing trend with the increase of laser power or the decrease of scanning speed, which indicates that the mechanical property of the laser-irradiated region is strongly dependent on the irradiation conditions. To quantitatively assess the mechanical property evolution induced by laser irradiation, the Meyer's hardness of the original RB-SiC surface and laser-irradiated regions was calculated utilizing the following equation

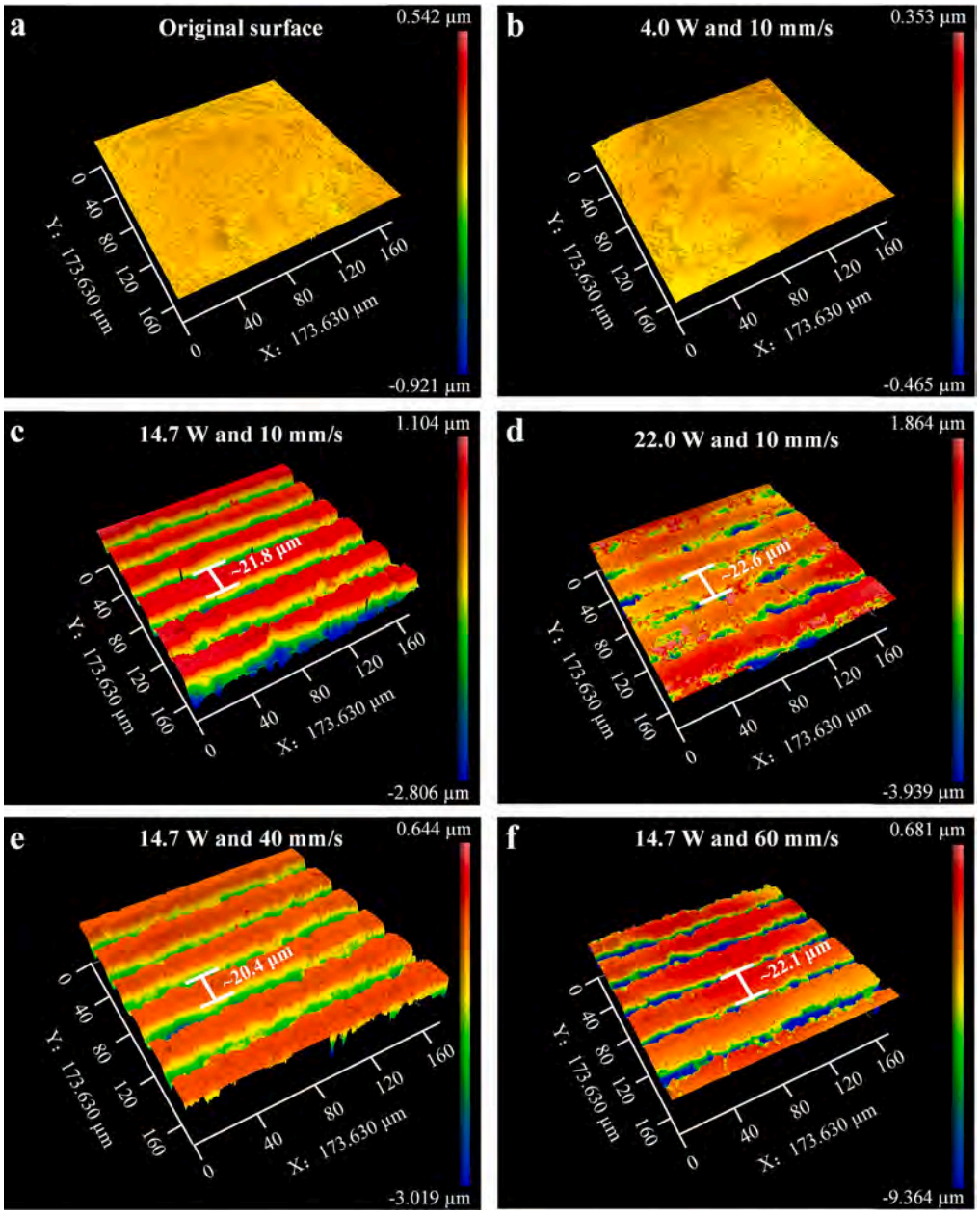

Fig. 4. 3D profiles of the (a) original RB-SiC surface and laser-irradiated regions (after polishing) obtained under different irradiation conditions: (b) 4.0 W and 10 mm/s, (c) 14.7 W and 10 mm/s, (d) 22.0 W and 10 mm/s, (e) 14.7 W and 40 mm/s, and (f) 14.7 W and 60 mm/s.

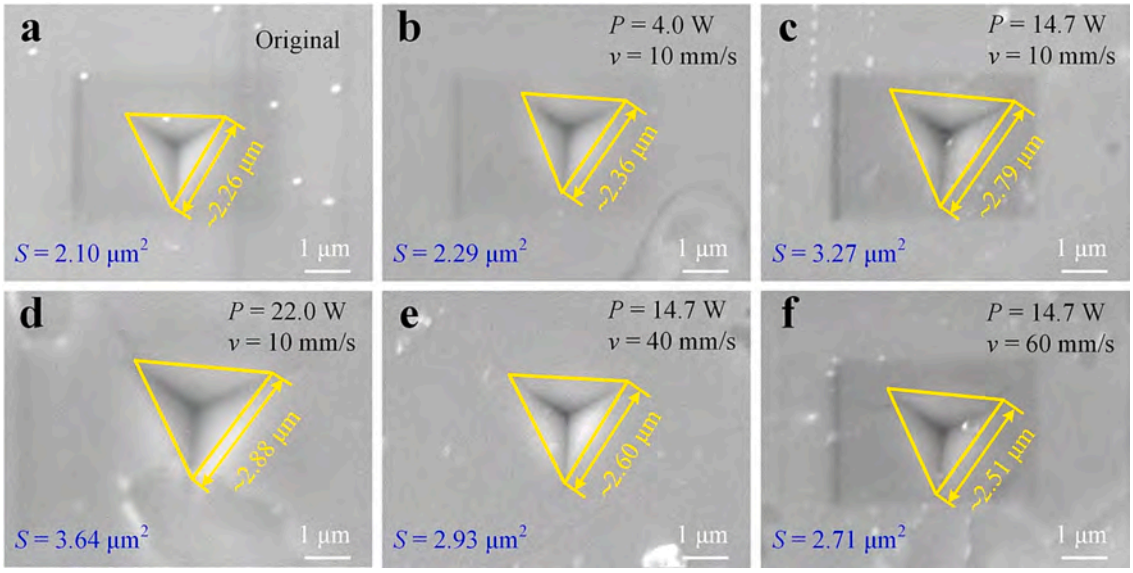

Fig. 5. SEM morphologies of the representative residual indents formed on the (a) original RB-SiC surface and laser-irradiated regions (after polishing) obtained under different irradiation conditions: (b) 4.0 W and 10 mm/s, (c) 14.7 W and 10 mm/s, (d) 22.0 W and 10 mm/s, (e) 14.7 W and 40 mm/s, and (f) 14.7 W and 60 mm/s.

[31]:

$$H = \frac{P_{max}}{A} \quad (1)$$

Where H represents Meyer's hardness, P_{max} denotes the maximum indentation load, and A stands for the projected area of the residual indent morphology. Fig. 7(a) and (b) depicts the statistical results of Meyer's hardness of the laser-irradiated regions obtained at different powers and scanning speeds, respectively. For comparison, the Meyer's hardness of the original RB-SiC surface is also included. The original RB-SiC surface has a relatively high Meyer's hardness of 22.42 GPa (see Fig. 7(a) and (b)), which is generally consistent with the results reported in the literatures [32,33]. After laser irradiation, the Meyer's hardness of the RB-SiC composite is decreased. In addition, the Meyer's hardness of the laser-irradiated region gradually decreases with the increase of laser power, and the relatively high laser power of 22.0 W results in a largest Meyer's hardness decrease of 9.12 GPa, i.e., softening degree reaches 40.7 % compared to the normal hardness of the original RB-SiC surface. As shown in Fig. 7(b), for the same laser power of 14.7 W, the Meyer's hardness of the laser-irradiated region gradually recovers from 14.37 GPa to 18.18 GPa when increasing the scanning speed from 10 mm/s to 60 mm/s, but it is still significantly lower than the Meyer's hardness of the original RB-SiC surface. The above results confirm that nanosecond pulsed laser irradiation is an effective strategy for reducing the surface hardness of RB-SiC composite, and the softening degree is strongly dependent on the laser irradiation conditions used.

3.2. Surface chemical composition

Based on the above analysis, it can be concluded that nanosecond laser irradiation can lead to a reduction in the hardness of RB-SiC composite. To investigate whether this hardness reduction is accompanied by the change in chemical composition, XRD tests were performed to compare the phase composition and content of the original RB-SiC surface and the polished laser-irradiated regions. Fig. 8(a) and (b) presents the XRD patterns of the laser-irradiated regions obtained at different powers and scanning speeds, respectively. For comparison, the XRD pattern of the original RB-SiC surface is also included. In Fig. 8(a) and (b), several sharp diffraction peaks corresponding to Si and SiC phases are present on the XRD patterns of both the original RB-SiC surface and the laser-irradiated regions obtained under different irradiation conditions, but there is a significant difference in the peak intensity. For the same laser scanning speed of 10 mm/s, the gradual increase in laser power leads to a gradual decrease of the peak intensity of SiC phases, while the Si content is the opposite, as illustrated in Fig. 8 (a). Similarly, for the same laser power of 14.7 W, decreasing the scanning speed from 60 mm/s to 10 mm/s also results in a gradual decrease of the peak intensity of SiC phases (see Fig. 8(b)). However, for Si phases, their content is essentially constant when varying the scanning speed, but they are still slightly higher than the Si content of the original RB-SiC surface. The results of Fig. 8(a) and (b) clearly indicate that nanosecond laser irradiation leads to the decomposition of SiC particles contained in the RB-SiC composite, and this effect is more pronounced with the increase of the input laser energy (i.e., increasing the laser power or decreasing the scanning speed) [34].

To further investigate possible elemental composition evolution induced by nanosecond laser irradiation, the elemental distribution characteristics of the laser-irradiated regions obtained at different scanning speeds were characterized by EDS, and the corresponding SEM-EDS mapping results are presented in Fig. 9(a). It can be qualitatively seen that the Si element is mainly concentrated in the smooth regions rather than in the laser scanning traces, while the C element is the opposite. This is further confirmed by the SEM-EDS line profiles shown in Fig. 9(b). Combined with the XRD patterns shown in Fig. 8 and the SEM-EDS results presented in Fig. 9, it can be concluded that the smooth regions used for nanoindentation tests mainly consist of Si phases, while the laser scanning traces are mainly enriched with SiC phases. In addition, it is worth noting that the diamond polishing paste used during the polishing process may remain in the low-lying laser scanning traces, further leading to the enrichment of C element in these regions [35].

3.3. Cross-sectional analysis

To investigate the evolution of subsurface characteristics of RB-SiC composite induced by nanosecond laser irradiation, the cross-sections of the original and laser-irradiated RB-SiC samples were obtained by diamond wire cutting, and then mechanically polished for subsequent micro-morphological observations, hardness tests, and chemical composition analysis. Fig. 10(a)-(f) presents the SEM morphologies of the cross-sections of the original and laser-irradiated RB-SiC samples. In

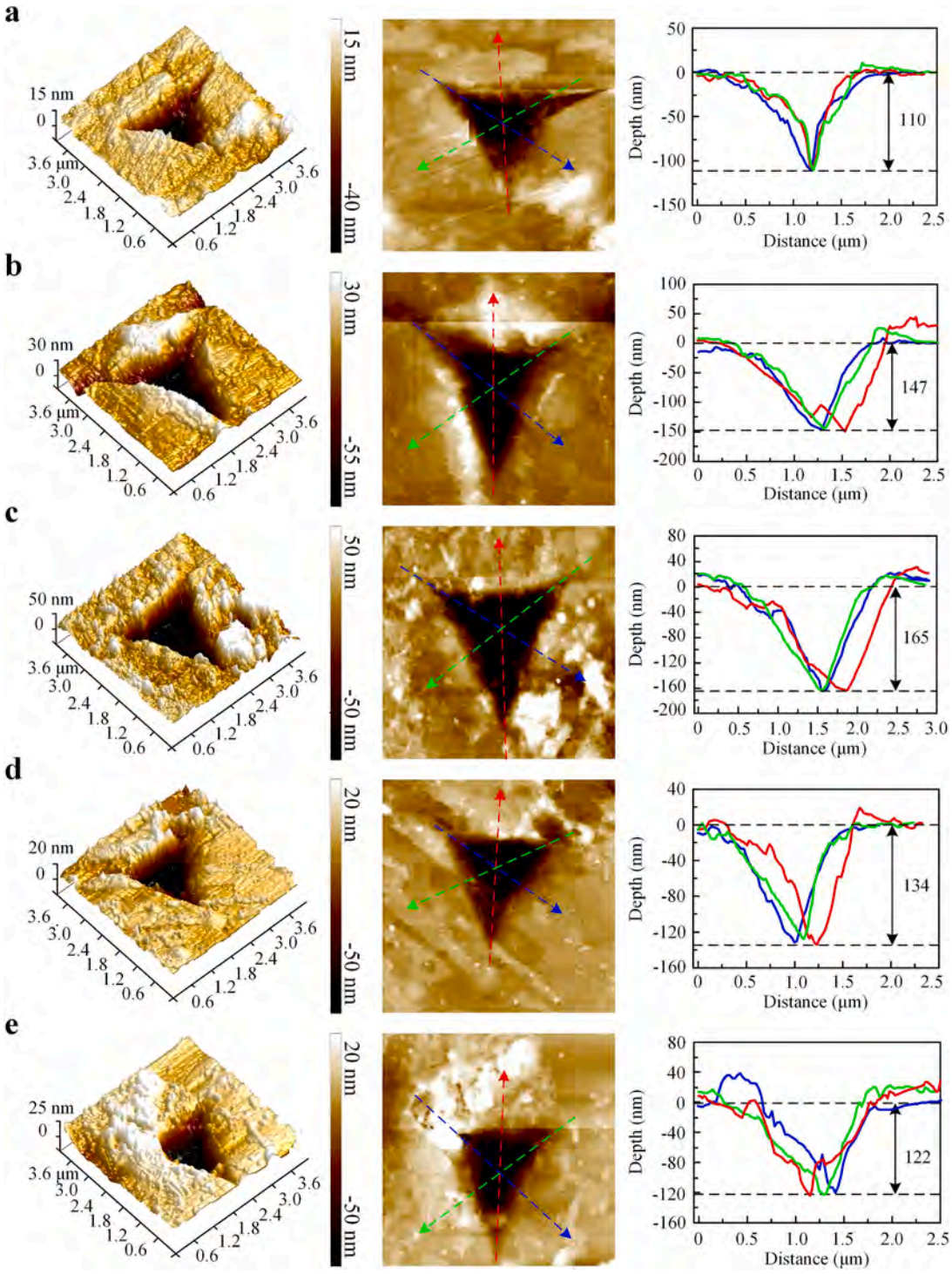

Fig. 6. AFM images of the representative residual indents formed on the laser-irradiated regions (after polishing) obtained under different irradiation conditions: (a) 4.0 W and 10 mm/s, (b) 14.7 W and 10 mm/s, (c) 22.0 W and 10 mm/s, (d) 14.7 W and 40 mm/s, and (e) 14.7 W and 60 mm/s.

the relatively low energy input regime (see Fig. 10(b)), the cross-sectional morphology of the laser-irradiated sample is similar to that of the original RB-SiC sample (see Fig. 10(a)), which is characterized by a relatively smooth surface. In contrast, in the relatively high energy input regime, micro-cone structures with a height of about tens of micrometres are observed, as illustrated in Fig. 10(c)-(f). The hardness distribution of the cross-sections of the original and laser-irradiated RB-SiC samples is presented in Fig. 10(g). It is seen that in the range of 0 to 80 μm away from the upper surface, the cross-sectional hardness of the laser-irradiated sample obtained at a relatively low laser power of 4.0 W fluctuates in the range of 22 to 25 GPa, which is basically consistent with that of the original RB-SiC composite. For laser-irradiated samples obtained at relatively high laser energy input regime, the hardness value shows a gradual increase trend with the increase of the distance from the upper surface, and then recovered to the hardness level of the original RB-SiC composite (i.e. 22 to 25 GPa) at 40 μm away from the upper surface. Combined with the XRD patterns presented in Fig. 8 and the SEM-EDS mapping results illustrated in Fig. 9, the decrease in hardness within the range of 0 to 40 μm away from the upper surface can be mainly attributed to the increase in the Si phase content.

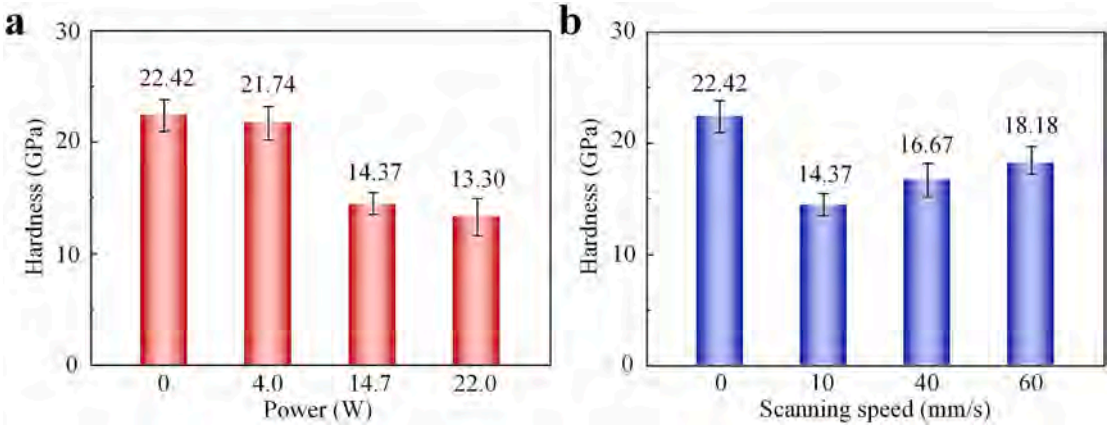

Fig. 7. The statistical results of Meyer's hardness of the laser-irradiated regions (after polishing) obtained at (a) different powers and (b) scanning speeds. For comparison, the Meyer's hardness of the original RB-SiC surface is also included.

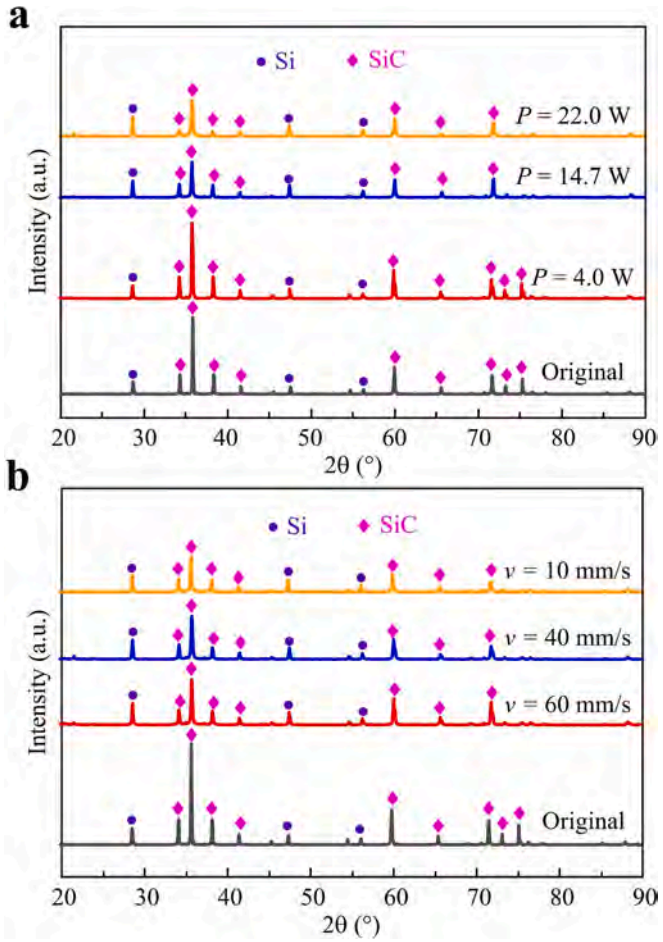

Fig. 8. XRD patterns of the laser-irradiated regions (after polishing) obtained at: (a) different powers and (b) scanning speeds. For comparison, the XRD pattern of the original RB-SiC surface is also included.

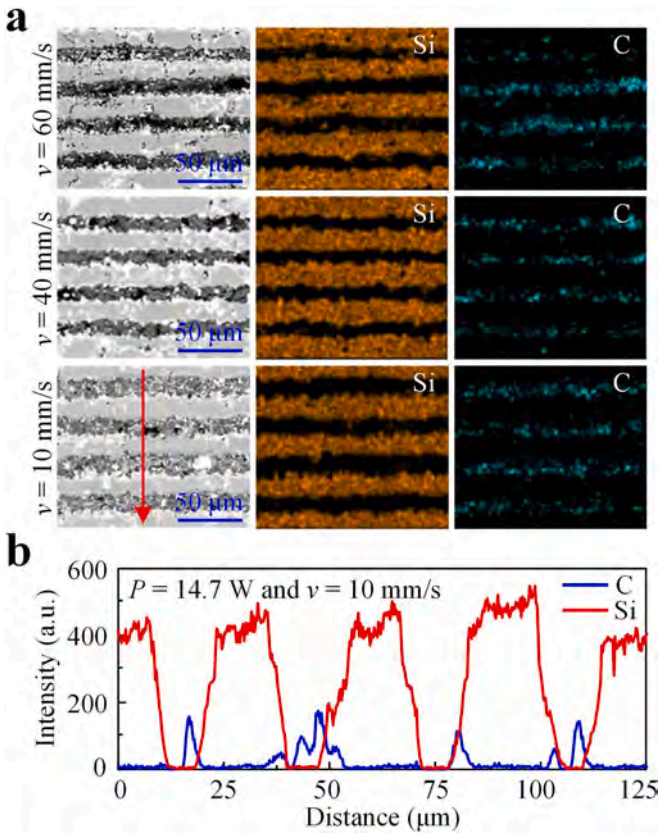

Fig. 9. (a) SEM-EDS mapping results of the laser-irradiated regions (after polishing) obtained at different scanning speeds. (b) Element distribution along the marked line in Fig. 9(a).

To further confirm the subsurface chemical composition evolution of RB-SiC composite induced by laser irradiation, EDS line scanning analysis were performed on the cross-sections of the original RB-SiC and laser-irradiated samples shown in Fig. 10(a)-(f), and the corresponding results are presented in Fig. 11. It is clearly seen that the Si and O elements are concentrated at the micro-cone structures generated at a laser power of 14.7 W and a laser scanning speed of 10 mm/s (see Fig. 11(c)), while the C element is the opposite, confirming that the micro-cone structures are mainly composed of Si and SiO_2. In particular, SiO_2 is amorphous and exists in the form of spider web-like film, as confirmed in our previous study [36].

3.4. Material removal behavior during the mechanical polishing process

The above results have indicated that nanosecond laser irradiation leads to surface softening of RB-SiC composite, which may enhance its removability. To confirm this, the weight loss of the original RB-SiC composite as well as laser-irradiated samples obtained under different irradiation conditions after 6 h of polishing treatment was obtained and

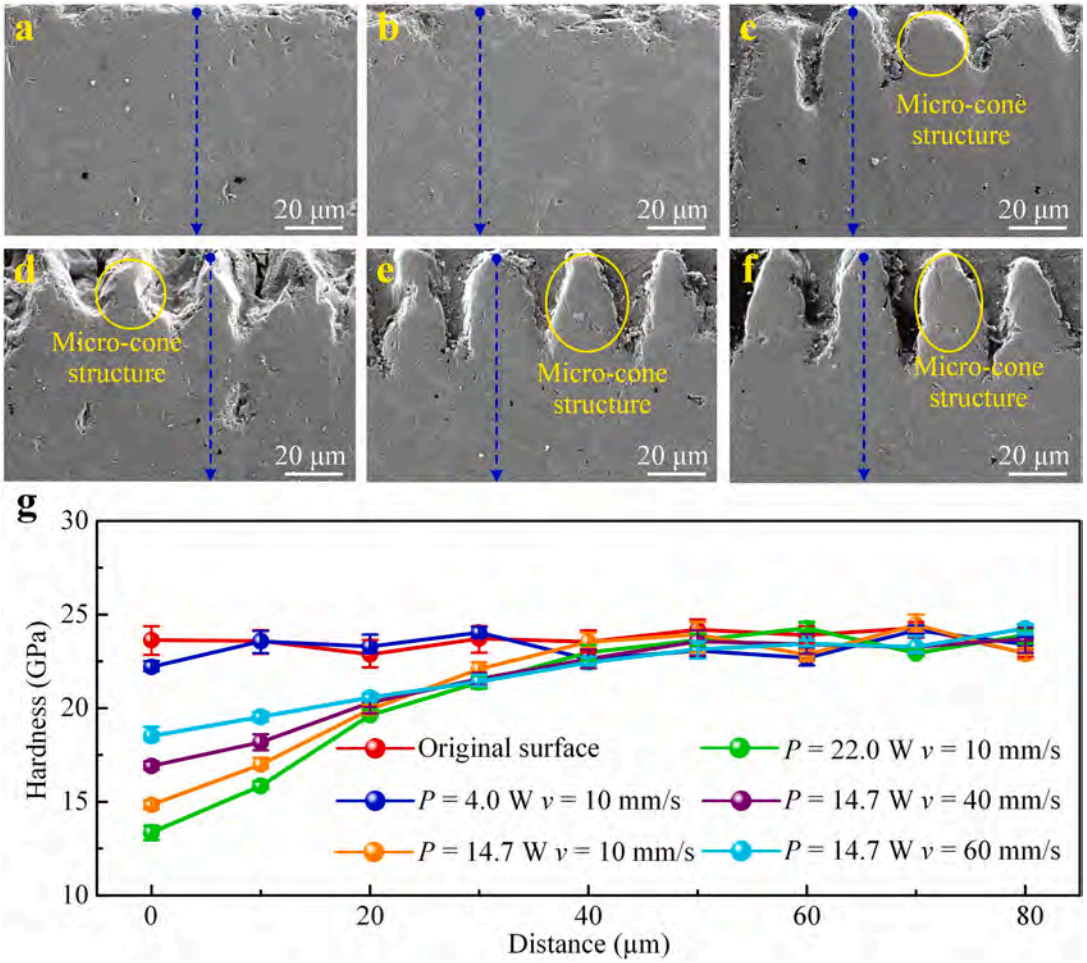

Fig. 10. SEM morphologies of the cross-sections of the (a) original RB-SiC and laser-irradiated samples obtained under various irradiation conditions: (b) 4.0 W and 10 mm/s, (c) 14.7 W and 10 mm/s, (d) 22.0 W and 10 mm/s, (e) 14.7 W and 40 mm/s, and (f) 14.7 W and 60 mm/s. (g) The cross-sectional hardness distribution of the original RB-SiC and laser-irradiated samples.

compared, and the results are presented in Fig. 12. To fundamentally understand the possible reason for the changes in removability, the weight loss of RB-SiC samples after laser irradiation under different irradiation conditions is also included. It is clearly seen that the weight loss of the original RB-SiC samples after laser irradiation tends to gradually increase as the laser power increases or the scanning speed decreases. After 6 h of polishing treatment, the weight loss of each laser-irradiated sample is higher than that of the original RB-SiC sample, implying a high removability of the laser-irradiated samples. In addition, the weight loss of the laser-irradiated samples after 6 h of polishing treatment exhibits an increasing trend when increasing the power from 4.0 W to 14.7 W or gradually decreasing the scanning speed from 60 mm/s to 10 mm/s, which is consistent with the hardness variation trend presented in Fig. 7(a) and (b). However, there is a discrepancy that when increasing the laser power from 14.7 W to 22.0 W, the hardness of the laser-irradiated sample and its weight loss after polishing are simultaneously reduced. This phenomenon may be due to the fact that more RB-SiC materials are removed after laser irradiation at a relatively high laser power of 22.0 W, resulting in the formation of a recast layer with a relatively small thickness [36]. More specifically, in the relatively high energy input regime, more molten materials dissipate into the air due to its initial kinetic energy, leading to a reduction in the thickness of the recast layer consisting of micro-cone structures, micro/nanoparticles, and spider web-like film.

To gain further insight into the reason for the change in removability, the removal behavior evolution of the laser-irradiated samples over the polishing time was comparatively investigated. Fig. 13(a) and (b) plots the change in weight loss of the laser-irradiated samples obtained under different powers and scanning speeds as a function of the polishing time, respectively. It is clearly seen that the slope of all the curves tends to decrease with the increase of polishing time, implying a gradual decrease in removability. In general, with the progress of mechanical polishing, the surface quality of the laser-irradiated samples will gradually improve, which can be responsible for the gradual reduction of the removability. To confirm this, the height variation of the micro-cone structures during the mechanical polishing process was monitored, and the corresponding results are shown in Fig. 14. It is clearly seen that the height of the micro-cone structures gradually decreases with the increase of polishing time, indicating that the recast structures are gradually removed and the laser-irradiated regions become flatter. Furthermore, the variations of surface roughness (*Sa*) of the laser-irradiated samples with polishing time were obtained, and the results are presented in Fig. 15. It is seen that the surface roughness (*Sa*) of the laser-irradiated samples shows a gradual decreasing trend with the increase of polishing time, that is, the laser-irradiated surfaces become flatter and flatter. This is further confirmed by the optical morphologies of the laser-irradiated samples after mechanical polishing for different times presented in Fig. 16, where the proportion of the smooth regions to the entire laser-irradiated region gradually increases with the increase of polishing time. An increase in the proportion of the smooth regions leads to an increase of the contact area between the laser-irradiated sample and the polishing block, and correspondingly, the local pressure will

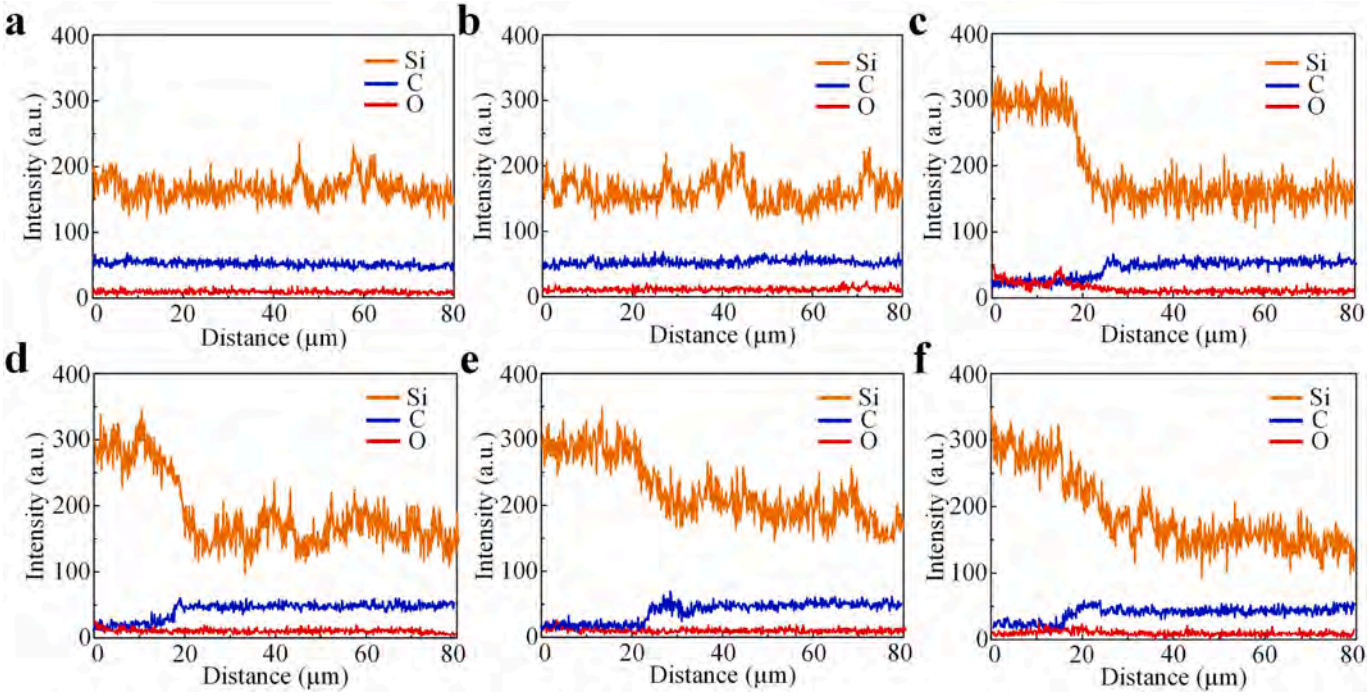

Fig. 11. (a)-(f) Elemental distribution along the marked lines in Fig. 10(a)-(f), respectively.

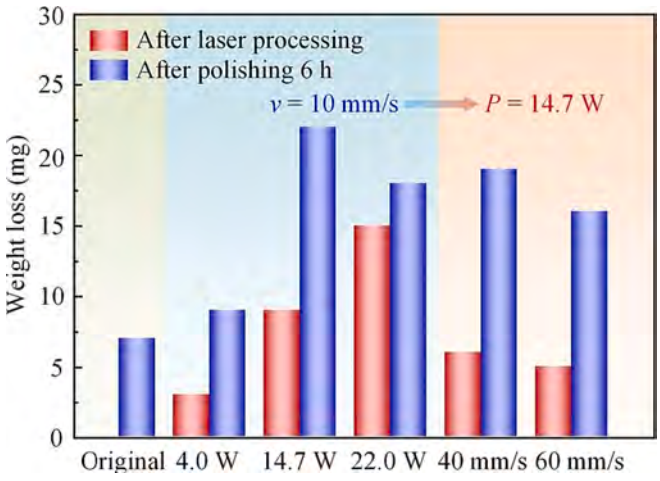

Fig. 12. Weight loss of the original RB-SiC sample as well as laser-irradiated samples obtained under different irradiation conditions after 6 h of polishing treatment. To fundamentally understand the possible reason for the change in removability, the weight loss of RB-SiC samples after laser irradiation under different irradiation conditions is also included.

decrease, which result in a reduction in removability [37].

3.5. The mechanism of changes in surface hardness and removability

To better modulate the surface characteristics of RB-SiC composite, understanding the underlying mechanisms of laser-induced changes in surface hardness and removability is the premise and foundation. Based on the above experimental results, it is found that the hardness of the laser-irradiated regions obtained under different irradiation conditions is lower than that of the original RB-SiC surface, and the softening degree strongly depends on the laser irradiation parameters used. To fundamentally understand the mechanism responsible for this softening phenomenon and its relevance to irradiation conditions, it is essential to gain insight into the interaction processes between laser and RB-SiC composite. To this end, the simulation analysis of the laser irradiation process was performed using COMSOL Multiphysics finite element software. The thermal physical parameters of the Si and SiC used in the simulations are summarized in Table 2.

Utilizing the thermal model proposed in Ref. [48], the temperature evolution of the homogeneous Si and SiC under nanosecond laser irradiation with various laser powers was analyzed, and the results are presented in Fig. 17. It is seen that with the increase of the laser power, the extent of heat accumulation on both Si and SiC surfaces is enhanced. In addition, as the number of laser pulses increases, the maximum temperature exhibits a gradual increasing trend due to the thermal accumulation effect.

Fig. 18(a) presents the schematic diagram of nanosecond laser ablation of RB-SiC composite. When a relatively low laser power of 4.0 W is employed, although the surface temperature of neither Si nor SiC does not exceed their respective melting temperatures (1440 K for Si and 2445 K for SiC), the surface temperature of SiC is significantly higher than the melting temperature of Si. In this case, only a small portion of the SiC particles experiences heating and melting, while the majority of the SiC particles are essentially unaffected. Moreover, in RB-SiC composite, the heat can be transferred from the SiC particles to the Si matrix due to its composite's structure, causing part of the Si matrix to melt. As a result, the laser-induced changes in the surface characteristics of RB-SiC composite are relatively weak, which is the reason why the laser-irradiated regions shown in Fig. 2(a) and 4(b) are relatively smooth without any obvious laser scanning traces. When the laser power is significantly increased to 14.7 or more, the surface temperatures of both Si and SiC exceeded their respective melting temperatures, and accordingly, a large number of SiC particles would be melted and decomposed at elevated temperatures, and the possible chemical reactions are shown below [49–52]:

$$SiC_{(solid)} \rightarrow Si_{(liquid)} + C_{(solid)} \quad (2)$$

$$C_{(solid)} + O_2 \rightarrow CO/CO_{2(gas)} \quad (3)$$

$$Si + O_2 \rightarrow SiO_2 \quad (4)$$

Accompanied by the decomposition of SiC particles, the molten pool

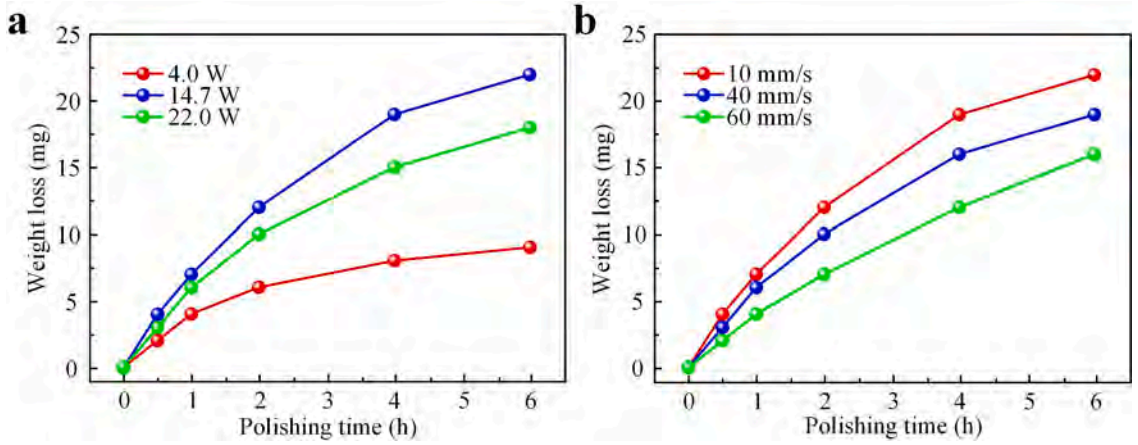

Fig. 13. Variations in weight loss of the laser-irradiated samples obtained under (a) different powers and (b) scanning speeds as a function of the polishing time.

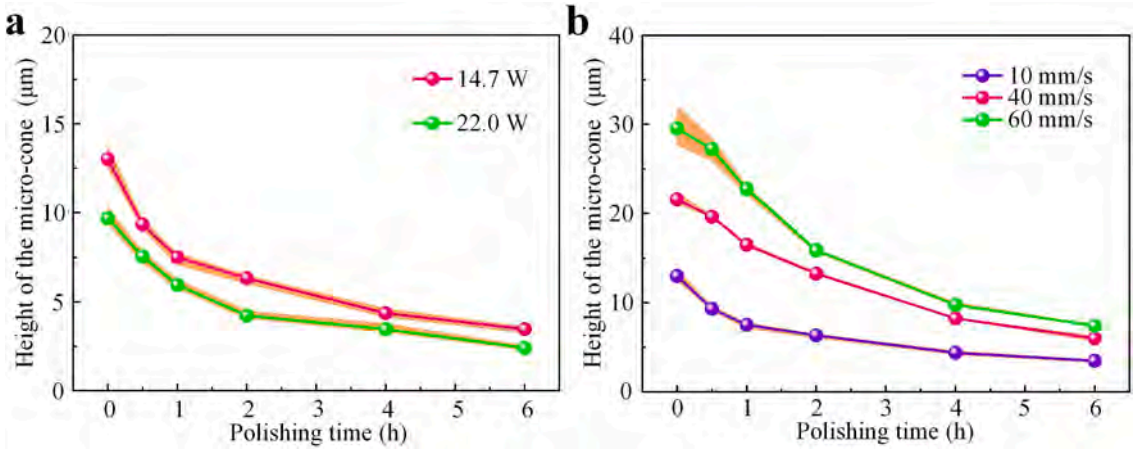

Fig. 14. Variations in height of the micro-cone structures generated under (a) different powers and (b) scanning speeds as a function of the polishing time.

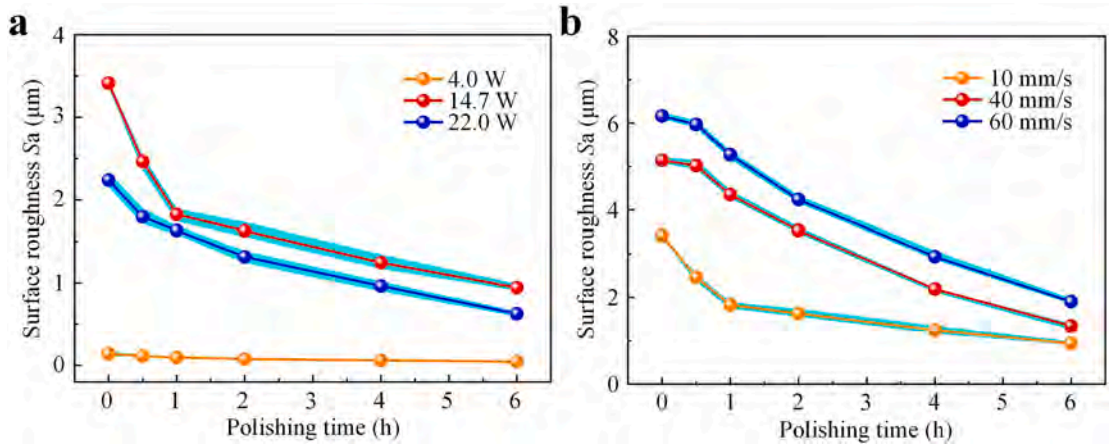

Fig. 15. Variations in surface roughness (*Sa*) of the laser-irradiated samples obtained under (a) different powers and (b) scanning speeds as a function of the polishing time.

composed mainly of liquid Si was formed on the top of the RB-SiC surface. With the action of the expanding plasma, recoil pressure and Marangoni convection [53–56], these molten Si would be moved from the center of the molten pool towards its edges, leading to the formation of micro-cone structures. Meanwhile, some evaporated Si vapour might react chemically with oxygen derived from air, and then fall back onto the RB-SiC surface under atmospheric pressure and gravity to form a spider web-like film mainly consisting mainly of amorphous SiO_2 [36]. Combining the SEM micrographs shown in Figs. 2 and 3, the XRD patterns illustrated in Fig. 8, and the elemental distribution results presented in Figs. 9 and 11, it can be summarised that the high-lying recast structures are mostly composed of Si. It is well known that the thermal and mechanical properties of the Si and SiC phases are quite different. In terms of surface hardness, Si phase is characterized by a

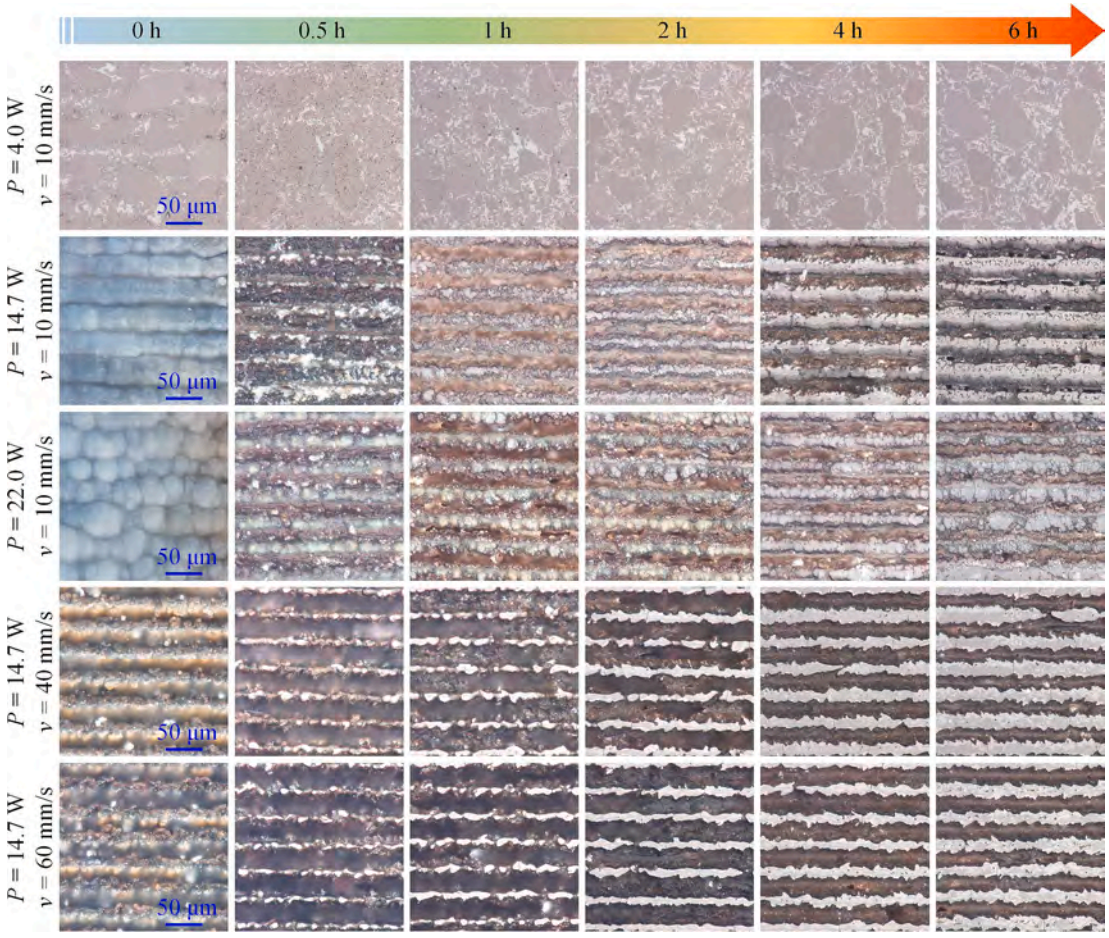

Fig. 16. Optical morphologies of the laser-irradiated samples after mechanical polishing for different times.

Table 2
The detailed thermal physical parameters of the Si and SiC.

Parameters	Si	SiC
Mass density ρ (kg/m^3)	2320 [38]	3100 [39]
Thermal conductivity k (W/(m·K)	0.7 [40]	0.1 [41]
Specific heat C_P (J/kg·K)	678 [40]	620 [41]
Latent heat of melting, L_m (J/kg)	1.79×10^6 [42]	1.3×10^5 [43]
Latent heat of vaporization, L_v (J/kg)	1.28×10^7 [42]	9.8×10^6 [43]
Emissivity	0.66 [42]	0.6 [43]
Melting point T_m (K)	1440 [40]	2445 [39]
Molar mass M (g/mol)	28.0 [44]	40.0 [45]
Coefficient of thermal expansion (1/K)	10.5×10^{-6} [46]	4×10^{-6} [47]

nanoindentation hardness in the range of 12 to 16 GPa [57], pales in comparison to the impressive nanoindentation hardness of SiC phase, which is measured at the range of 32 to 36 GPa [58]. This is the main reason for surface softening of RB-SiC composite induced by laser irradiation. In addition, combined with the statistical results of Meyer's hardness shown in Fig. 7 and the XRD patterns presented in Fig. 8, it is observed that an increase in the peak intensity of Si phases is always accompanied by a decrease in the hardness, which further confirms the significant correlation between the Si contents of the laser-irradiated regions and their hardness.

The experimental results show that compared with the original RB-SiC sample, the weight loss of the laser-irradiated samples after mechanical polishing is relatively high. To explain the high removability of the laser-irradiated samples, a schematic diagram illustrating the material removal behavior of the laser-irradiated sample during the mechanical polishing process is presented in Fig. 18(b). As mentioned earlier, the most significant reason for the enhanced removability of RB-SiC composite after laser irradiation can be attributed to the laser-induced recast structures with a relatively low hardness, which are easier to remove during the mechanical polishing process compared to the original RB-SiC sample. In addition, the spider web-like film covered on the micro-cone structures is loose and porous, which can be easily removed by scraping or even touching. Another reason responsible for the high removability of the laser-irradiated samples may be their non-uniform geometrical profiles. Combined with Figs. 2 and 3, it is observed that the topography of the laser-irradiated surfaces is full of ups and downs, and the recast structures on both sides of the laser scanning traces are high-lying compared to the laser-irradiated scanning traces. Therefore, during the mechanical polishing process, the recast structures on both sides of the laser scanning traces bear all the pressure of the polishing block, i.e., the direct contact area between the laser-irradiated surface and polishing block is significantly smaller than that between the original RB-SiC surface and the polishing block, which leads to a higher localized pressure and thus facilitates the removal of the surface materials. Overall, the high removability of the laser-irradiated samples is attributed to a combination of their lower surface hardness and non-uniform geometric profiles.

4. Conclusions

In summary, the RB-SiC composite was irradiated by a nanosecond pulsed laser with different laser irradiation parameters in an atmospheric environment, and the influence of laser irradiation conditions on the surface characteristics and removability of the laser-irradiated regions was comprehensively investigated. Based on the experimental

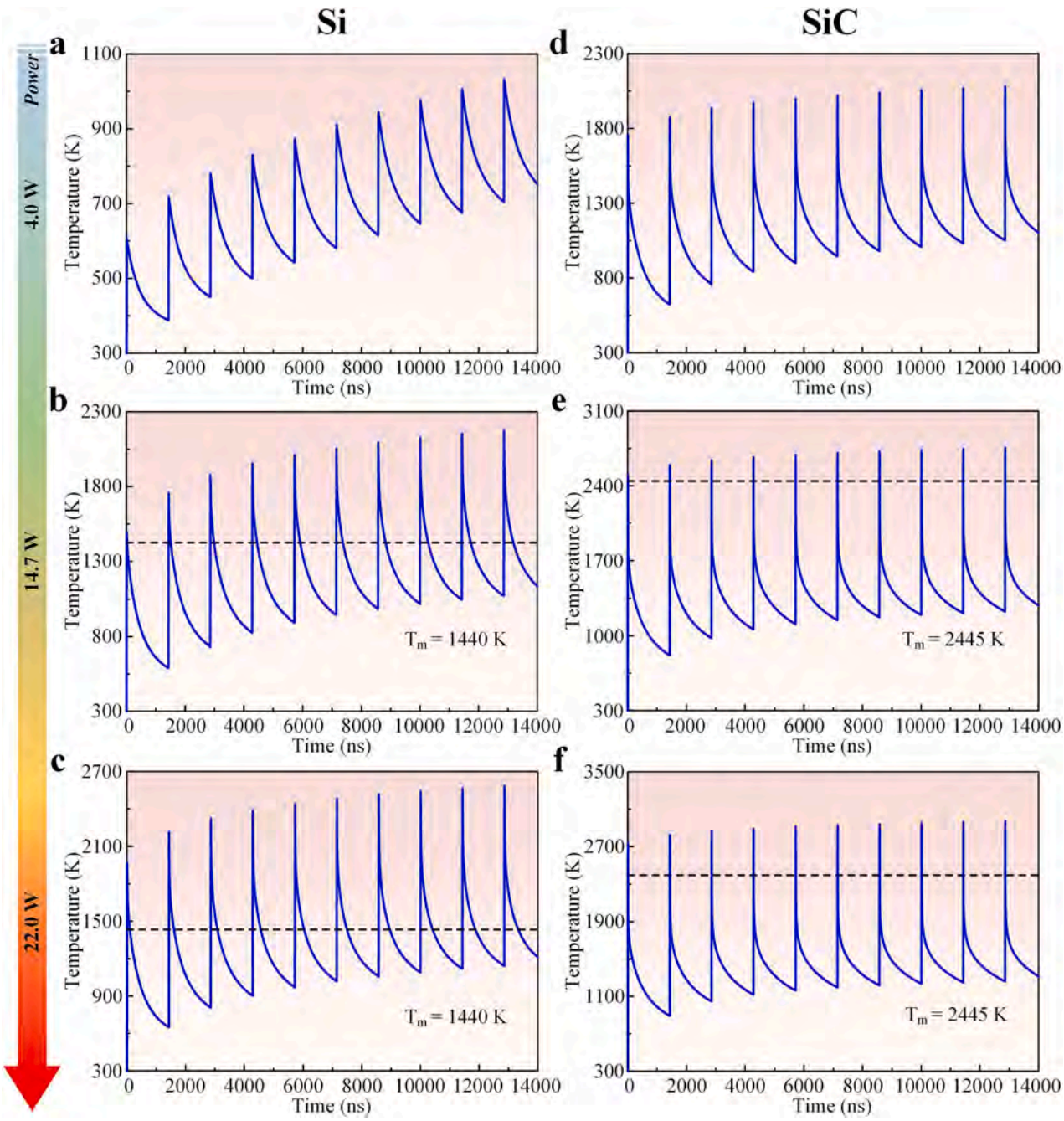

Fig. 17. Temperature evolution of the homogeneous (a)-(c) Si and (d)-(f) SiC under nanosecond laser irradiation with various laser powers.

results, the main conclusions can be summarized as follows:

(1) Nanosecond laser irradiation could effectively soften the RB-SiC composite, and the softening degree was strongly dependent on the laser irradiation parameters. Increasing the laser power or decreasing the scanning speed resulted in a reduction in the hardness of the laser-irradiated region. In particular, the minimum hardness value of the laser-irradiated region reached 13.30 GPa, which is 40.7 % lower than that of the original RB-SiC surface (22.42 GPa).

(2) The chemical composition analysis indicated that after laser irradiation, the peak intensity of the SiC phases was decreased while the Si content was increased, which was responsible for the hardness reduction of RB-SiC composite.

(3) The removability of the laser-irradiated samples is higher than that of the original RB-SiC sample, owing to their relatively low hardness and non-uniform geometric profiles.

The present study demonstrates the feasibility of nanosecond pulsed laser irradiation as a promising technique for improving the removability of RB-SiC composite, which contributes to the development of advanced thermal-assisted setups/methods for achieving efficient processing of RB-SiC composite.

Data availability statement

The data that support the findings of this study are available from the corresponding author upon reasonable request.

CRediT authorship contribution statement

Hong An: Data curation, Formal analysis, Investigation, Software, Validation, Visualization, Writing – original draft. **Yongfeng Qian:**

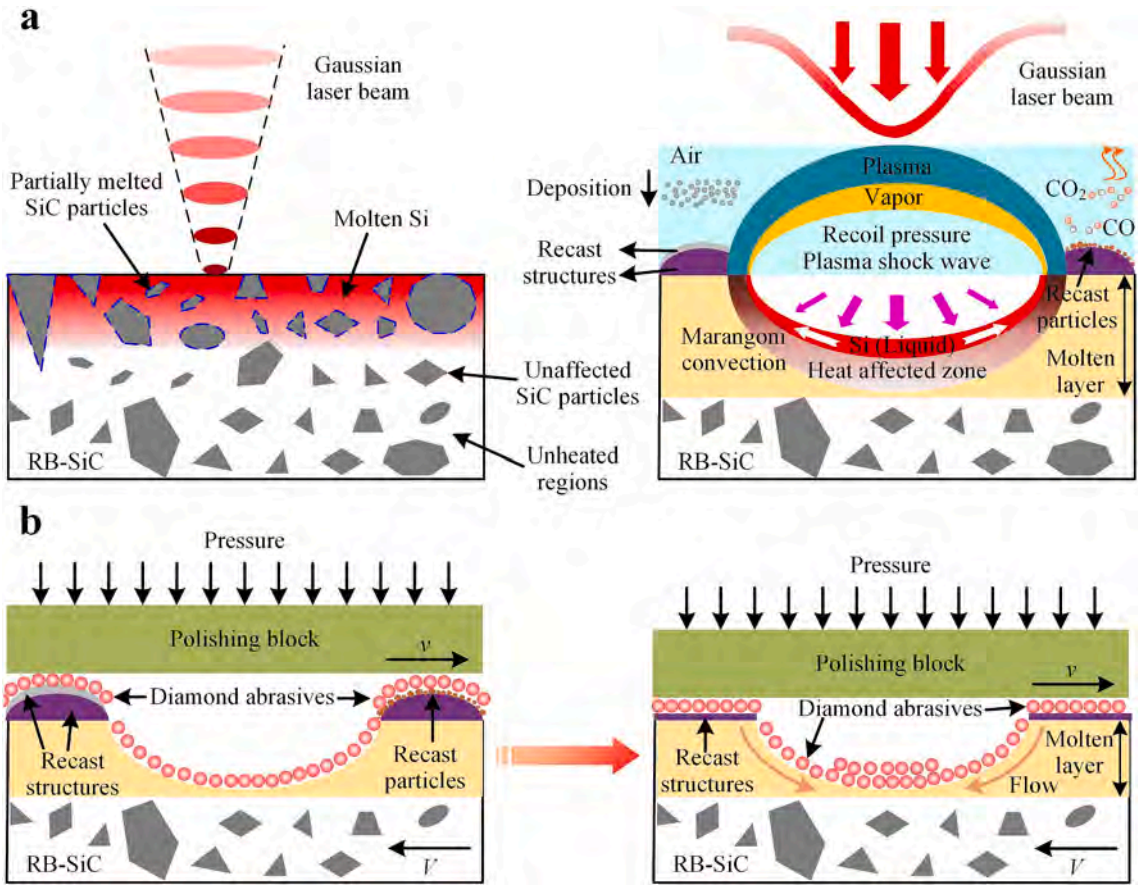

Fig. 18. Schematic diagram illustrating (a) the interaction processes between laser and RB-SiC composite as well as (b) the material removal behavior of the laser-irradiated RB-SiC sample during the mechanical polishing process.

Formal analysis, Funding acquisition, Investigation, Project administration, Validation, Visualization, Writing – review & editing. **Lin Zhang:** Data curation, Investigation. **Zhiyu Zhang:** Data curation, Investigation, Resources. **Hu Huang:** Conceptualization, Funding acquisition, Investigation, Methodology, Project administration, Supervision, Writing – review & editing. **Jiwang Yan:** Supervision.

Declaration of competing interest

The authors declare that they have no known competing financial interests or personal relationships that could have appeared to influence the work reported in this paper.

Data availability

Data will be made available on request.

Acknowledgements

This work was supported by the Natural Science Foundation of Jilin Province (20220101198JC), the National Key Research and Development Plan Project (Grant No. 2022YFB4600204), the China Postdoctoral Science Foundation (GZB20230256), the Scientific Research Projects of the Education Department of Jilin Province (Grant No. JJKH20241256KJ), the Graduate Innovation Fund of Jilin University (Grant No. 2023CX062), the Opening Project of the Key Laboratory of CNC Equipment Reliability, Ministry of Education, Jilin University (JLU-cncr-202306), and the Fundamental Research Funds for the Central Universities (2023-JCXK-02).

References

[1] Shimamura A, Katsui H, Zhou Y, Hotta M, Kondo N, Fukushima M. Improvement in fracture strength of porous reaction-bonded silicon carbide with unique surface layer by incorporating α-silicon carbide powder as a secondary phase. J Eur Ceram Soc 2022;42(13):5458–63.
[2] Zhang N-L, Yang J-F, Deng Y-C, Wang B, Yin P. Preparation and properties of reaction bonded silicon carbide (RB-SiC) ceramics with high SiC percentage by two-step sintering using compound carbon sources. Ceram Int 2019;45(12):15715–9.
[3] Chen H, Wei C, Cao Z, Peng X, Jiang Z, Wan S, et al. Improving polishing efficiency of RB-SiC through femtosecond laser pretreatment. Appl Surf Sci 2023;631:157574.
[4] Hu Y. Feasibility of using wet abrasive jet machining to produce flat and crack-free micro-textures on reaction bonded silicon carbide. J Mater Process Tech 2022;300:117423–40.
[5] Rao X, Zhang F, Xu J. Wheel wear behavior and its influence on grinding performance in electrical discharge diamond grinding of reaction-bonded silicon carbide. J Manuf Process 2023;85:904–14.
[6] Zhang Z, Yao P, Wang J, Huang C, Zhu H, Liu H, et al. Nanomechanical characterization of RB-SiC ceramics based on nanoindentation and modelling of the ground surface roughness. Ceram Int 2020;46(5):6243–53.
[7] Rao X, Zhang F, Lu Y, Luo X, Ding F, Li C. Analysis of diamond wheel wear and surface integrity in laser-assisted grinding of RB-SiC ceramics. Ceram Int 2019;45(18):24355–64.
[8] Zou Y, Li C-H, Tang Y, Hu L, Liu J-A, Wu J-M, et al. Preform impregnation to optimize the properties and microstructure of RB-SiC prepared with laser sintering and reactive melt infiltration. J Eur Ceram Soc 2020;40(15):5186–95.
[9] Zhang J, Han L, Zhang J, Liu H, Yan Y, Sun T. Brittle-to-ductile transition in elliptical vibration-assisted diamond cutting of reaction-bonded silicon carbide. J Manuf Process 2019;45:670–81.
[10] Huangfu Y, Ruan K, Qiu H, Lu Y, Liang C, Kong J, et al. Fabrication and investigation on the PANI/MWCNT/thermally annealed graphene aerogel/epoxy electromagnetic interference shielding nanocomposites. Compos A Appl Sci Manuf 2019;121:265–72.
[11] An Q, Chen J, Ming W, Chen M. Machining of SiC ceramic matrix composites: A review. Chinese J Aeronaut 2021;34(4):540–67.

[12] Marathe U, Padhan M, Bijwe J. Carbon nanotubes- A powerful nano-filler for enhancing the performance properties of polyetherketoneketone composites and adhesives. Compos Sci Technol 2021;210:108813–24.
[13] Ghosh G, Sidpara A, Bandyopadhyay PP. High efficiency chemical assisted nanofinishing of HVOF sprayed WC-Co coating. Surf Coat Tech 2018;334:204–14.
[14] Pang M, Wu Y, Wang Z, Wang S, Ding Y, Ma L, et al. Effect of ethylenediamine on the surface glazed phenomenon of fixed abrasive pad under deionized water condition. Int J Adv Manuf Technol 2023;128(3-4):1049–61.
[15] Liu Q, Liao Z, Axinte D. Temperature effect on the material removal mechanism of soft-brittle crystals at nano/micron scale. Int J Mach Tool Manu 2020;159:103620–35.
[16] Liu Q, Chen M, Liao Z, Feng J, Xu D, Cheng J. On the improvement of the ductile removal ability of brittle KDP crystal via temperature effect. Ceram Int 2021;47(23):33127–39.
[17] Zhang S, Li Z, Yao Y, Tian L, Yan Y. Heat transfer characteristics and compatibility of molten salt/ceramic porous composite phase change material. Nano Energy 2022;100:107476–85.
[18] Aoki T, Ogasawara T. Tyranno ZMI fiber/$TiSi_2$–Si matrix composites for high-temperature structural applications. Compos A Appl Sci Manuf 2015;76:102–9.
[19] Li N, Liu W, Xiong H, Qin R, Huang S, Zhang G, et al. In-situ reaction of Ti-Si-C composite powder and formation mechanism of laser deposited Ti6Al4V/ (TiC+Ti_3SiC_2) system functionally graded material. Mater Design 2019;183:108155.
[20] Harder BJ. Oxidation performance of Si-H_fO_2 environmental barrier coating bond coats deposited via plasma spray-physical vapor deposition. Surf Coat Tech 2020;384:125311–8.
[21] Javid M, Qu X, Huang F, Li X, Farid A, Shah A, et al. In-situ synthesis of SiC/Fe nanowires coated with thin amorphous carbon layers for excellent electromagnetic wave absorption in GHz range. Carbon 2021;171:785–97.
[22] Lim SJ, Cheon J, Kim M. Effect of laser surface treatments on a thermoplastic PA 6/carbon composite to enhance the bonding strength. Compos A Appl Sci Manuf 2020;137:105989–98.
[23] Denkena B, Krödel A, Grove T. Influence of pulsed laser ablation on the surface integrity of PCBN cutting tool materials. Int J Adv Manuf Technol 2018;101(5–8):1687–98.
[24] Wang J, Cao L, Zhang Y, Liu Y, Fang H, Chen J. Effect of mass transfer channels on flexural strength of C/SiC composites fabricated by femtosecond laser assisted CVI method with optimized laser power. J Adv Ceram 2021;10(2):227–36.
[25] Zhang C, Li Z, Li H, Yang Q, Wang H, Shan C, et al. Femtosecond Laser-Induced Supermetalphobicity for Design and Fabrication of Flexible Tactile Electronic Skin Sensor. ACS Appl Mater Interfaces 2022;14(33):38328–38.
[26] Qian Y, Jiang M, Zhang Z, Huang H, Hong J, Yan J. Microstructures and mechanical properties of Zr-based metallic glass ablated by nanosecond pulsed laser in various gas atmospheres. J Alloy Compd 2022;901:163717–25.
[27] Chen Y-D, Liu H-Y, Cheng C-Y, Chen C-C. Comparison of C face (0001) and Si face (0001) of silicon carbide wafers in femtosecond laser irradiation assisted chemical–mechanical polishing process. Appl Phys A 2022;128(12):1094–102.
[28] Yan G, Lu S, Zhang M, Wang J, Yang X, Zhang Z, et al. Wear and corrosion behavior of P20 steel surface modified by gas nitriding with laser surface engineering. Appl Surf Sci 2020;530:147306.
[29] Deb SK, Wilding M, Somayazulu M, McMillan PF. Pressure-induced amorphization and an amorphous - Amorphous transition in densified porous silicon. Nature 2001;414(6863):528–30.
[30] Qin X, Li X, Chen X, Yang X, Zhang F, Xu X, et al. Raman scattering study on phonon anisotropic properties of SiC. J Alloy Compd 2019;776:1048–55.
[31] Hong J, Qian Y, Zhang L, Huang H, Jiang M, Yan J. Laser nitriding of Zr-based metallic glass: An investigation by orthogonal experiments. Surf Coat Tech 2021;424:127657–67.
[32] Nguyen T, Liu D, Thongkaew K, Li H, Qi H, Wang J. The wear mechanisms of reaction bonded silicon carbide under abrasive polishing and slurry jet impact conditions. Wear 2018;410–411:156–64.
[33] Rao X, Zhang F, Luo X, Ding F. Characterization of hardness, elastic modulus and fracture toughness of RB-SiC ceramics at elevated temperature by Vickers test. Mater Sci Eng, A 2019;744:426–35.
[34] Xue G, Ke L, Zhu H, Liao H, Zhu J, Zeng X. Influence of processing parameters on selective laser melted SiCp/AlSi10Mg composites: Densification, microstructure and mechanical properties. Mater Sci Eng, A 2019;764:138155–64.
[35] Huang H, Qian Y, Zhang L, Jiang M, Yan J. A novel method for fabricating micro-dimple arrays with good surface quality on metallic glass substrate by combining laser irradiation and mechanical polishing under wax sealing. J Manuf Process 2022;79:911–23.
[36] An H, Qian Y, Zhang L, Zhang Z, Huang Hu, Yan J. Fabrication and functional characteristics of micro/nano structures on the RB-SiC surface through nanosecond pulsed laser irradiation. Ceram Int 2023;49(22):36276–88.
[37] Yang H, Xie J, He Q, Liu J, Shi Y. Study on diamond cutting-to-burnishing for thermal-force dispersion in dry metal grinding. J Mater Process Tech 2023;313:117874–87.
[38] Shen X, Hsiao P-C, Wang Z, Liu M, Phua B, Song N, et al. Modelling picosecond and nanosecond laser ablation for prediction of induced damage on textured SiNx/Si surfaces of Si solar cells. Prog Photovolt 2021;29(9):1020–33.
[39] Zhang H, Li C, Zhang L, Men G, Ning H. Effect of laser pulse energy deposition method on nanosecond laser scanning ablation of SiCp/AA2024 composites. J Manuf Process 2022;83:695–704.
[40] Son Y, Shin J. Experimental and numerical study of Si annealed by laser sources of the visible spectrum (red and blue wavelength). Vacuum 2023;215:112364–76.
[41] Dutto C, Fogarassy E, Mathiot D. Numerical and experimental analysis of pulsed excimer laser processing of silicon carbide. Appl Surf Sci 2001;184(1-4):362–6.
[42] Tangwarodomnukun V, Wang J, Huang CZ, Zhu HT. Heating and material removal process in hybrid laser-waterjet ablation of silicon substrates. Int J Mach Tool Manu 2014;79:1–16.
[43] Zhang R, Wang Q, Huang C, Wang J, Tang A, Zhao W. Energy Transfer Between Femtosecond Laser and Silicon Carbide. JOM 2023;75(9):4047–58.
[44] Rienitz O, Pramann A, Vogl J, Lee K-S, Yim Y-H, Malinovskiy D, et al. The comparability of the determination of the molar mass of silicon highly enriched in 28Si: results of the CCQM-P160 interlaboratory comparison and additional external measurements. Metrologia 2020;57(6):065028.
[45] Zheng L, Fang C, Zeng C, Luo X, Zhang Ze, Zhang X, et al. Microstructure, mechanical and anti-ablation properties of Mg-modified C/C–ZrC–SiC composites prepared by sol-gel technology. Ceram Int 2022;48(23):34728–42.
[46] Arsha AG, Manoj V, Akhil MG, Anbukkarasi R, Rajimol PR, Rajan TPD. Squeeze infiltration processing and characterization of silicon reinforced composites. Mater Today Commun 2022;32:103870–9.
[47] Yu Q, Romagnoli A, Al-Duri B, Xie D, Ding Y, Li Y. Heat storage performance analysis and parameter design for encapsulated phase change materials. Energ Convers Manage 2018;157:619–30.
[48] Hong J, Huang H, Zhang L, Zhang Z, Jiang M, Yan J. Laser polishing and simultaneous hardening of the electrical discharge machined Zr-based metallic glass surface. Mater Design 2024;237:112599–616.
[49] Zhai Z, Wang W, Zhao J, Mei X, Wang K, Wang F, et al. Influence of surface morphology on processing of C/SiC composites via femtosecond laser. Compos A Appl Sci Manuf 2017;102:117–25.
[50] Xu X, Luan X, Zhang J, Cao X, Zhao D, Cheng L, et al. Significant improvement of ultra-high temperature oxidation resistance of C/SiC composites upon matrix modification by SiH_fBCN ceramics. Compos B Eng 2023;253:110553.
[51] Das M, Balla VK, Kumar TSS, Bandyopadhyay A, Manna I. Tribological, electrochemical and in vitro biocompatibility properties of SiC reinforced composite coatings. Mater Design 2016;95:510–7.
[52] Wu L, Li Y, Zhou B, Liu J, Cheng D, Guo S, et al. Vertical graphene on rice-husk-derived SiC/C composite for highly selective photocatalytic CO_2 reduction into CO. Carbon 2023;207:36–48.
[53] Qian Y, Jiang M, Zhang Z, Huang H, Yan J. On the transformation between micro-concave and micro-convex in nanosecond laser ablation of a Zr-based metallic glass. J Manuf Process 2021;68:1114–22.
[54] Qian M, Goh CS, Sun YH, Ng FL. Effects of CNTs on microstructure and hardness of laser welds of the CNT-reinforced magnesium composite. Compos A Appl Sci Manuf 2013;48:67–72.
[55] Gu D, Zhang H, Dai D, Xia M, Hong C, Poprawe R. Laser additive manufacturing of nano-TiC reinforced Ni-based nanocomposites with tailored microstructure and performance. Compos B Eng 2019;163:585–97.
[56] Gu D, Hagedorn Y-C, Meiners W, Wissenbach K, Poprawe R. Nanocrystalline TiC reinforced Ti matrix bulk-form nanocomposites by Selective Laser Melting (SLM): Densification, growth mechanism and wear behavior. Compos Sci Technol 2011;71(13):1612–20.
[57] Jarząbek DM, Milczarek M, Nosewicz S, Bazarnik P, Schift H. Size Effects of Hardness and Strain Rate Sensitivity in Amorphous Silicon Measured by Nanoindentation. Metall Mater Trans A 2020;51(4):1625–33.
[58] Eswar Prasad K, Ramesh KT. Hardness and mechanical anisotropy of hexagonal SiC single crystal polytypes. J Alloy Compd 2019;770:158–65.